

IRS-Assisted Ambient Backscatter Communications Utilizing Deep Reinforcement Learning

Xiaolun Jia, *Student Member, IEEE*, and Xiangyun Zhou, *Senior Member, IEEE*

Abstract—We consider an ambient backscatter communication (AmBC) system aided by an intelligent reflecting surface (IRS). The optimization of the IRS to assist AmBC is extremely difficult when there is no prior channel knowledge, for which no design solutions are currently available. We utilize a deep reinforcement learning-based framework to jointly optimize the IRS and reader beamforming, with no knowledge of the channels or ambient signal. We show that the proposed framework can facilitate efficient AmBC communication with a detection performance comparable to several benchmarks under full channel knowledge.

Index Terms—Ambient backscatter communication, intelligent reflecting surface, deep reinforcement learning.

I. INTRODUCTION

Ambient backscatter communication (AmBC) is a key enabler for highly energy-efficient, pervasive networking for the Internet of Things, where an AmBC device (or tag) conveys information on top of an already modulated radiofrequency (RF) signal [1]. Despite the research activity surrounding AmBC, its robustness remains as a key obstacle to be addressed. The information-bearing backscattered signal at the reader experiences severe direct-link interference from the ambient signal, which may be unknown and is several orders of magnitude stronger, thus resulting in poor detection performance. As a result, currently AmBC only supports either very short ranges, or relatively low data rates.

Various methods have been proposed to improve the detection performance of AmBC, such as transceiver design, channel estimation, and modifications to network infrastructure. Work in [2] proposed a tag capable of performing frequency shift modulation to separate the backscattered signal from the direct-link interference, at the cost of tag implementation complexity. Detection algorithms based on channel estimation and machine learning methods were presented in [3], [4]. Recently, the use of an intelligent reflecting surface (IRS) to improve AmBC performance has also been proposed, with exploratory studies presented in [5], [6].

IRSs have received significant research interest due to their ability to impose reconfigurable phase shifts on impinging signals to obtain desired reception at a receiver. The joint phase shift optimization of a large number of reflecting elements allow favorable received signal strength scaling, proportional to the IRS surface area [7]. A further advantage of individually reconfigurable phase shifts is the ability to focus signals in different directions to reduce inter-user interference [8].

The authors are with the School of Engineering, The Australian National University, Canberra, Australia.

E-mail: {xiaolun.jia, xiangyun.zhou}@anu.edu.au.

This advantage makes IRS an ideal candidate to address the problem of severe direct-link interference in the AmBC system, and hence improve AmBC detection performance without requiring modification of the tags.

In this letter, we study the signaling design and phase shift optimization of an IRS-assisted AmBC system. Due to the unknown, varying nature of the ambient signal and the difficulty of estimating the IRS-tag channels, we assume that the channel state information (CSI) is not available. To our best knowledge, such a scenario has not been addressed before. Work in [9] is the only existing study on the joint optimization of AmBC and IRS, but nonetheless under the assumption of full CSI; while work in [3] optimizes the AmBC detection without CSI, but in a system with no IRS. We solve the optimization problem using a DRL-based approach, namely the deep deterministic policy gradient (DDPG) algorithm. The lack of CSI also differentiates the problem formulation and our version of the DDPG algorithm from those used in conventional IRS-assisted systems with known CSI [10]–[12]. Our results indicate that the proposed approach performs comparably to several benchmarks with full CSI knowledge.

II. SYSTEM MODEL AND PROBLEM FORMULATION

Consider an AmBC system in Fig. 1 with an ambient RF source, a single-antenna tag, an IRS with N reflectors and a reader with M antennas. Hereafter, we assign subscripts S , T , I and R to the source, tag, IRS and reader, respectively.

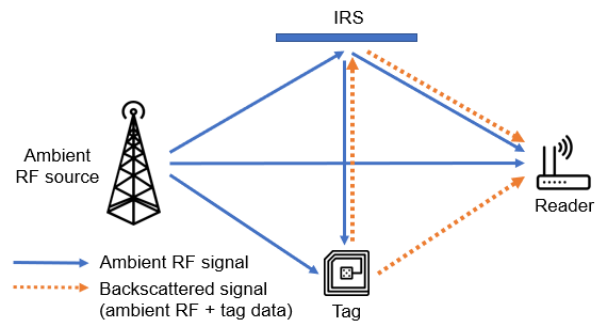


Fig. 1: IRS-assisted AmBC system.

We adopt a discrete-time signal model, as in [13]. The source transmits signal $s[\ell]$, whose samples are i.i.d. and follow $\mathcal{CN}(0, P_S)$, where P_S is the transmit power. The assumption of a complex Gaussian ambient signal is commonly adopted in AmBC systems [3], [13], [14].

The tag is equipped with two impedances and performs on-off keying (OOK) modulation, with the data symbols being

either 0 or 1. For ease of exposition, we assume that the tag has a built-in battery. As the tag acts as a diffuse scatterer, we take the strengths of signal paths undergoing two or more reflections at the tag before reaching the reader to be negligible. However, this assumption does not apply at the IRS, due to its ability to enhance the overall signal strength while balancing between different reflection links.

Linear combining is assumed at the reader, using the vector $\mathbf{g} \in \mathbb{C}^{M \times 1}$, where we set $\|\mathbf{g}\|^2 = 1$ without loss of generality. Conventional energy detection [3] is utilized to recover the backscattered data symbols after applying the combiner.

Denote the channels from the source to tag, source to IRS, source to reader, tag to reader, tag to IRS and IRS to reader by $\mathbf{h}_{ST} \in \mathbb{C}^{1 \times 1}$, $\mathbf{h}_{SI} \in \mathbb{C}^{N \times 1}$, $\mathbf{h}_{SR} \in \mathbb{C}^{M \times 1}$, $\mathbf{h}_{TR} \in \mathbb{C}^{M \times 1}$, $\mathbf{h}_{TI} \in \mathbb{C}^{N \times 1}$ and $\mathbf{h}_{RI}^H \in \mathbb{C}^{M \times N}$, respectively. Frequency-flat quasi-static fading is assumed for all channels. Moreover, we assume that the reader has no knowledge of the ambient signal or the CSI of any channel in the system.

Each IRS reflector has a reconfigurable phase shift, denoted by $\theta_n \in [0, 2\pi)$ for the n -th reflector. The sum of incident signals at each reflector is subject to the reflection coefficient Θ_n arising from the phase shift, with $\Theta_n = e^{j\theta_n}$. The amplitude scaling of all IRS reflectors is set to unity. Thus, the matrix of reflection coefficients at the IRS can be written as $\Theta = \text{diag}(\Theta_1, \dots, \Theta_N)$.

The signal received by the tag, consisting of the direct source-tag and reflected source-IRS-tag signal paths, is

$$y_T[\ell] = (\mathbf{h}_{TI}^H \Theta \mathbf{h}_{SI} + h_{ST}) s[\ell]. \quad (1)$$

The backscattered signal is given by

$$x_T[\ell] = \alpha b[\ell] y_T[\ell], \quad (2)$$

where α denotes the tag splitting coefficient, which is set to 1 without loss of generality; and $b[\ell]$ denotes the ℓ -th sample of the backscattered data symbol. We assume that the duration of one backscatter symbol spans L samples. Therefore, denoting the k -th backscatter symbol as b_k , we have $b[\ell] = b_k \in \{0, 1\}, \forall \ell \in \{(k-1)L+1, \dots, kL\}$.

The reader receives the ambient RF signal from the source-reader and source-IRS-reader paths, plus the backscattered signals from four paths, as combinations of {source-tag, source-IRS-tag} multiplied by {tag-reader, tag-IRS-reader} paths:

$$\mathbf{y}_R[\ell] = \begin{cases} \mathbf{h}_0 s[\ell] + \mathbf{z}_R[\ell], & b[\ell] = 0, \\ (\mathbf{h}_0 + \alpha \mathbf{h}_1) s[\ell] + \mathbf{z}_R[\ell], & b[\ell] = 1, \end{cases} \quad (3)$$

with $\mathbf{h}_0 = \mathbf{H}_{RI}^H \Theta \mathbf{h}_{SI} + \mathbf{h}_{SR}$ and $\mathbf{h}_1 = (\mathbf{H}_{RI}^H \Theta \mathbf{h}_{TI} + \mathbf{h}_{TR}) \times (\mathbf{h}_{TI}^H \Theta \mathbf{h}_{SI} + h_{ST})$, where $\mathbf{z}_R[\ell] \sim \mathcal{CN}(0, P_w \mathbf{I})$ is the noise at the reader. The final signal after the combiner is given by $\mathbf{g}^H \mathbf{y}_R$. We adopt the shorthand $\mathbf{h}_A \triangleq \mathbf{h}_0$, $\mathbf{h}_I \triangleq \alpha \mathbf{h}_1$ and $\mathbf{h}_{AI} \triangleq \mathbf{h}_A + \mathbf{h}_I$, where subscripts A and I represent the ambient and information-bearing components, respectively.

As per conventional AmBC systems (e.g., [14]), the energies of the received 0 and 1 symbols are modeled as Gaussian random variables, with means and variances given by

$$\mu_0 = P_s |\mathbf{g}^H \mathbf{h}_A|^2 + P_w, \quad \sigma_0^2 = \mu_0^2 / L, \quad (4)$$

$$\mu_1 = P_s |\mathbf{g}^H (\mathbf{h}_A + \alpha \mathbf{h}_I)|^2 + P_w, \quad \sigma_1^2 = \mu_1^2 / L. \quad (5)$$

We define the *generalized relative channel difference (GRCD)* as $\Delta_G = \max \left\{ \frac{\mu_1}{\mu_0}, \frac{\mu_0}{\mu_1} \right\}$, which is the energy ratio between the symbol with the higher energy and the symbol with the lower energy. We note that the GRCD directly determines the BER of the AmBC system. Under a central limit theorem assumption and reasonably large L , the BER is derived from [3] as

$$p_b = \frac{1}{2} \left[Q_N \left(\sqrt{L} \left(\frac{\Delta_G \log \Delta_G}{\Delta_G - 1} - 1 \right) \right) + Q_N \left(\sqrt{L} \left(1 - \frac{\log \Delta_G}{\Delta_G - 1} \right) \right) \right], \quad (6)$$

where $Q_N(\cdot)$ is the Gaussian Q -function. Hence, one can show that the BER reduces as the GRCD increases.

In this letter, we aim to maximize the GRCD of the IRS-assisted AmBC system as a substitute for minimizing the BER, by jointly designing the IRS reflection coefficients and the reader's combiner. The problem can be written as

$$(P) : \max_{\mathbf{g}, \Theta} \Delta_G \quad (7a)$$

$$\text{s.t.} \quad 0 \leq \theta_n \leq 2\pi, \forall n \in \{1, \dots, N\}, \quad (7b)$$

$$\|\mathbf{g}\|^2 = 1. \quad (7c)$$

Note that Δ_G in Problem (P) can only be obtained when the full CSI is available. As our work assumes the absence of CSI, we propose a DRL-based solution in the next section, by approximating Δ_G based on instantaneous signal observations.

III. DRL-BASED FRAMEWORK

A. Reinforcement Learning Fundamentals

Reinforcement learning (RL) problems concern the interactions between an agent and the environment in order to maximize a reward. This interaction can be formulated as a Markov decision process (MDP). At each time step t , the state s_t characterizes the environment. Based on s_t , the agent takes an action a_t drawn from a policy π . The action influences the environment, which takes on a new state s_{t+1} ; while a reward r_t is provided to the agent based on s_t and a_t . The agent accumulates experience over time through such interactions to learn the characteristics of the environment. Each interaction generates an experience $\langle s_t, a_t, r_t, s_{t+1} \rangle$, which is stored by the agent. The agent aims to determine an optimal policy $\pi_* : \mathcal{S} \rightarrow \mathcal{A}$ to maximize the action-value function and thus the expected long-term discounted reward (return), given by

$$Q_\pi(s_t, a_t) = \mathbb{E} \left\{ \sum_{k=0}^{\infty} \gamma^k r_{t+k+1} \mid s_t = s, a_t = a \right\}, \quad (8)$$

where $\gamma \in [0, 1]$ denotes the discount factor. The updating of Q_π to obtain the optimal policy is known as Q -learning. DNN-based methods have been proposed to approximate the Q -function. However, the main drawback of Q -learning is that it is only suitable for discrete state and action spaces.

DDPG is an algorithm sharing similarities with Q -learning that is applicable to problems with continuous action spaces [15]. Two components, namely the actor and critic, simultaneously learn the policy and Q -functions, respectively. Both actor and critic consist of two DNNs, termed the training and target nets. When presented with an experience stored in the agent's memory, the training actor net determines the next

action based on its parameterized policy. The action is then evaluated by the training critic net, which gradually learns a better approximation of the Q -function. The target actor and critic nets are also gradually updated based on their respective training nets to improve convergence. The DDPG architecture is shown in Fig. 2.

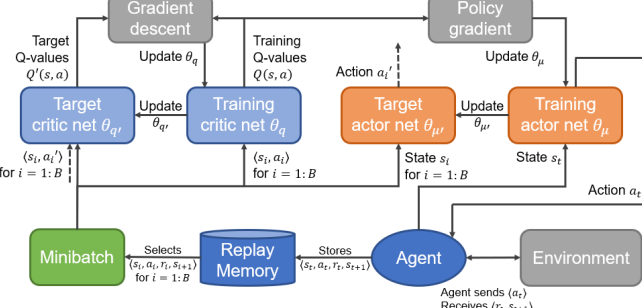


Fig. 2: Diagram of the DDPG algorithm.

Denote the parameters (weights) of the training and target actor nets by θ_μ and $\theta_{\mu'}$, respectively, and those of the training and target critic nets by θ_q and $\theta_{q'}$, respectively. Here, we use the notation $\mu(s_t)$ instead of π to denote the policy, to highlight the continuous action space. The agent stores past experiences in its replay memory \mathcal{E} . At each time step, the agent samples a minibatch of B experiences from \mathcal{E} and computes target Q -values for each experience by

$$y_i = r_i + \gamma Q'(s_{i+1}, \mu'(s_{i+1}|\theta_{\mu'})|\theta_{q'}), \quad (9)$$

where $Q'(s, a)$ is the Q -value from the target critic net. Next, gradient descent optimization is performed on the parameters of the training critic net to minimize the overall loss between the target Q -values and those produced by the training net, with the loss function given by

$$\mathcal{L}(\theta_q) = \frac{1}{B} \sum_{i=1}^B (y_i - Q(s_i, a_i|\theta_q))^2. \quad (10)$$

Subsequently, the training actor net, which produces the agent's policy, is updated by sampling the policy gradient (PG), which provides an approximation of the policy's expected return. Maximizing the return involves performing gradient ascent, whose update rule is given by

$$\theta_{k+1} = \theta_k + \alpha_\mu \nabla_a Q(s_t, \mu(s_t|\theta_\mu)|\theta_q) \nabla_{\theta_\mu} \mu(s_t|\theta_\mu), \quad (11)$$

where α_μ is the learning rate, and the subsequent terms approximate the PG. Finally, to ensure stability during training, the target nets are updated every T_{up} time steps according to

$$\theta_{a'} = \tau \theta_a + (1 - \tau) \theta_{a'}, \quad a \in \{\mu, q\}, \quad (12)$$

where $\tau \ll 1$ is the update coefficient for the target nets.

B. DRL Problem Reformulation and Proposed Algorithm

Problem (P) can be formulated as an MDP, where the reader acts as the agent and is responsible for the joint design of the IRS reflection coefficients and its own combiner as its action. This is achieved by interacting with the wireless propagation environment, which is characterized by the channels.

Each channel coherence period, consisting of T time steps, is defined as one episode. Due to the stochastic and unknown nature of the channels, each episode is independent from others, as the underlying environment varies with the channels in each episode. Thus, a key difference of the DRL framework in our work compared to existing DRL works involving IRS (e.g., [10]–[12]), where the CSI is known, is the fact that the actor and critic are trained in each episode based only on the observations in the current episode. The state, action and reward are defined as follows:

- **State:** The current state is defined as the concatenation of the previous combiner IRS reflection coefficients. As existing DNN implementations do not support complex inputs, the real and imaginary components of combiner weights and reflection coefficients are used:

$$s_t = [\text{Re}\{[g_1^{(t-1)}, \dots, g_M^{(t-1)}, \Theta_1^{(t-1)}, \dots, \Theta_N^{(t-1)}]\}, \text{Im}\{[g_1^{(t-1)}, \dots, g_M^{(t-1)}, \Theta_1^{(t-1)}, \dots, \Theta_N^{(t-1)}]\}]. \quad (13)$$

In total, there are $2M+2N$ elements in each observation.

- **Action:** The action space consists of the real and imaginary components of only the updated reflection coefficients based on the current state, for reasons which will be explained in the sequel. That is,

$$a_t = [\text{Re}\{[\Theta_1^{(t)}, \dots, \Theta_N^{(t)}]\}, \text{Im}\{[\Theta_1^{(t)}, \dots, \Theta_N^{(t)}]\}]. \quad (14)$$

As such, there are $2N$ elements to each action.

- **Reward:** Instead of using the GRCD directly as the reward, we use a modified reward function, given by $r_t = 100(\Delta_G^{(t)} - 1)$. Note that $\Delta_G^{(t)}$ is defined as the estimated ("sample") GRCD at time step t based on the received samples within the time step, and is elaborated in the sequel. From our experimentation, we observed that when random combiner weights and reflection coefficients are used, the majority of GRCD values are close to 1, which may lead to underfitting when different states and actions result in similar rewards. The multiplicative factor of 100 thus spreads out the reward space, such that each reward may be relatively more distinct, allowing faster convergence to be achieved by the critic nets.

In our experimentation with various state and action spaces, we observed poor performance when the combiner and reflection coefficients were set together. Thus, inspired by [3], we propose to pre-set the combiner to the optimal eigenvector beamformer corresponding to the signal observations in the current DRL step, independent from the reflection coefficients (which are updated later). This has two practical advantages. First, the optimal combiner results in a relatively large GRCD (compared to e.g., a random combiner), which can be further improved through tuning the reflection coefficients. Second, the Q -function, which relies on both state and action, is derived from only one combiner, as opposed to one from the current state and one from the action (which may be vastly different), resulting in more effective fitting of the Q -function.

The T time steps in each episode are divided into training and data transmission phases. In the training phase, each step is a DRL agent-environment interaction, and consists of two

pairs of backscatter pilot symbols, with each pair being a 0 followed by a 1, and each symbol spanning L_t samples. The estimated channel covariance matrices for the first pilot pair, denoted by \mathbf{C}_i , $i \in \{0, 1\}$, are first obtained using the current reflection coefficients (i.e., $\Theta^{(t-1)}$), and given by

$$\mathbf{C}_i = \frac{1}{L_t} \sum_{\ell=1}^{L_t} \mathbf{y}_R[\ell] \mathbf{y}_R[\ell]^H |_{b_k=i}, \quad (15)$$

and are then refined using its maximum eigenvalue and corresponding eigenvector [3]. Then, we update the combiner by solving the equation $\mathbf{C}_1 \mathbf{g} = \lambda \mathbf{C}_0 \mathbf{g}$, where λ represents the generalized eigenvalues of $\{\mathbf{C}_0, \mathbf{C}_1\}$. The combiner is set to the eigenvector of the maximum eigenvalue λ^+ if $\lambda^+ > 1/\lambda^-$, with λ^- being the minimum eigenvalue, and the eigenvector for λ^- otherwise. The updated combiner is then concatenated with the current IRS reflection coefficients to give an ‘intermediate’ state $s_{t,\text{int}}$. We then feed this intermediate state into the actor to obtain the updated reflection coefficients, which is the action for this DRL step. The second pair of pilot symbols is then transmitted, yielding \mathbf{C}'_i , $i \in \{0, 1\}$, and refined similarly. The sample GRCD for the current DRL step is then obtained by evaluating $\Delta_G^{(t)} = \max \left\{ \frac{\mathbf{g}^H \mathbf{C}'_1 \mathbf{g}}{\mathbf{g}^H \mathbf{C}'_0 \mathbf{g}}, \frac{\mathbf{g}^H \mathbf{C}'_0 \mathbf{g}}{\mathbf{g}^H \mathbf{C}'_1 \mathbf{g}} \right\}$.

As the underlying channels are unknown, we reserve the first T_{train} time steps of each episode, where the agent utilizes DRL and explores while training the actor and critic to learn the environment and its reward function. The T_{train} steps are further divided into two phases: in the first phase, the agent takes random actions for T_1 steps; while in the second phase, the agent takes actions generated from its policy network for T_2 steps. After T_{train} steps, the final set of reflection coefficients and combiner weights is fixed for the remainder of the episode, which is the data transmission phase, where a shorter symbol duration of L_d samples is used to provide a higher data rate. We note that the use of a training phase is critical to achieve desirable results for this problem.

The complete process is summarized in Algorithm 1.

IV. NUMERICAL RESULTS

We demonstrate the performance of the DRL framework in this section. The channels between the IRS and the source, tag and reader are assumed to undergo Rician fading as in [9], with Rician factor 3; while all other channels experience Rayleigh fading. The path loss exponent is 2.5 for all channels. The ambient signal frequency is 2.4 GHz with transmit power $P_s = 20$ dBm. The source, tag, IRS and reader are located at $[-5, 0]$, $[0, 0]$, $[0, 5]$ and $[5, 0]$ m, respectively. The reader has $M = 4$ antennas and the noise variance is $P_w = -95$ dBm. Without loss of generality, we group sub-groups of IRS reflectors to take on the same reflection coefficients for efficient computation [16], such that each effective reflector is one-wavelength-sized.

The training and target nets in the actor and critic are all four-layer fully-connected DNNs, with an input layer, two hidden layers and an output layer. The number of neurons in the actor and critic nets are $[2M + 2N, 4M + 4N, 4M + 4N, 2N]$ and $[2M + 4N, 4M + 8N, 4M + 8N, 1]$, respectively. The

Algorithm 1 DDPG Algorithm for Joint Reflection and Beamforming Design

- 1: **Inputs:** Replay memory \mathcal{E} ; minibatch size B ; actor and critic learning rates, α_μ and α_q ; update coefficient for target nets, τ ; discount factor, γ ; noise process \mathcal{N}
- 2: **for** each episode **do**
- 3: Initialize training actor and critic nets $\mu(s|\theta_\mu)$ and $Q(s, a|\theta_q)$; target actor and critic nets $\mu'(s|\theta_{\mu'}) = \mu(s|\theta_\mu)$ and $Q'(s, a|\theta_{q'}) = Q(s, a|\theta_q)$; random initial values $\mathbf{g}^{(0)}$ and $\Theta^{(0)}$; empty replay memory \mathcal{E}
- 4: **for** time step $t = 1:T_{\text{train}}$ **do**
- 5: Observe \mathbf{C}_0 and \mathbf{C}_1 and set $\mathbf{g}^{(t)}$ to the optimal eigenvector beamformer
- 6: Set intermediate state $s_{t,\text{int}} \leftarrow \{\mathbf{g}^{(t)}, \Theta^{(t-1)}\}$
- 7: Observe \mathbf{C}'_0 and \mathbf{C}'_1 . **If** $t < T_1$ then take random action; **else** take action $a_t = \mu(s_{t,i}|\theta_\mu) + \mathcal{N}$
- 8: Set next state $s_{t+1} \leftarrow \{\mathbf{g}^{(t)}, a_t\}$ and store experience $\langle s_t, a_t, r_t, s_{t+1} \rangle$ in \mathcal{E}
- 9: Sample a minibatch \mathcal{B} of B experiences from \mathcal{E}
- 10: Set target Q -values for minibatch \mathcal{B} according to (9)
- 11: Perform gradient descent on training critic net by minimizing loss function in (10)
- 12: Update training actor net using sampled PG in (11)
- 13: Update target actor and critic nets according to (12)
- 14: Update state $s_t \leftarrow s_{t+1}$
- 15: **end for**
- 16: **end for**

hidden layers use the rectified linear unit (ReLU) activation function; while a linear activation is applied to the output layer. Following the linear activation, each pair of outputs from the actor nets, corresponding to one reflection coefficient, is ℓ_2 -normalized to attain unit magnitude. The parameters for the DNNs are $\alpha_\mu = \alpha_q = 0.002$, $\tau = 0.0005$, $T_{\text{up}} = 1$, $B = 16$; and the optimizer is RMSprop with momentum 0.8. The noise process \mathcal{N} for the policy is the Ornstein-Uhlenbeck process with standard deviation 0.05. 1000 channel realizations are used, with $\{T_1, T_2\} = \{1000, 500\}$ steps, and $\gamma = 0$ [11]. The characteristics of the reward function, such as the maximum attainable reward, varies with each channel realization. This behavior is unique to our problem when the CSI is unknown. In order for the critic nets to properly fit the reward function for each channel realization, the Q -values must be based on the instantaneous reward, resulting in zero discount factor.

Fig. 3 highlights the effect of the number of IRS reflectors on the GRCD and BER, in the training and data transmission phases, respectively. For this experiment, random samples of $s[\ell]$ and $\mathbf{z}_R[\ell]$ are generated in each backscatter symbol period. The symbol durations for the training and data transmission phases are $\{L_t, L_d\} = \{150, 20\}$, with a larger L_t needed to accurately estimate the channel covariance matrices in (15). In addition from the results obtained using Algorithm 1, four benchmarks are included for comparison, which are: 1) the optimal zero-forcing (ZF) and 2) eigenvector (EIG) combiners when no IRS is present, 3) the optimal ZF combiner with

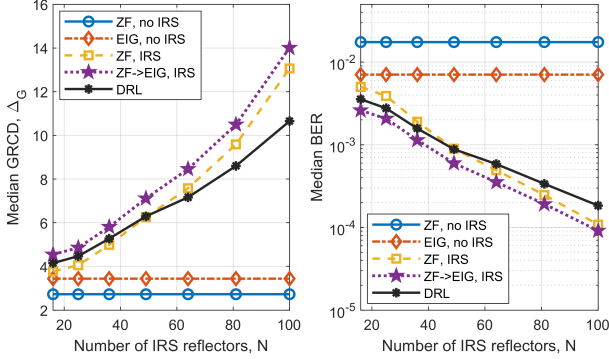


Fig. 3: (a) Median GRCD vs. N ; (b) Median BER vs. N .

IRS, and 4) the optimal EIG combiner with IRS, initialized using the optimal \mathbf{g} and Θ from 3). All four benchmarks are obtained under full CSI. Due to the large variance in GRCD values as a result of small-scale fading, the median GRCD is shown for each IRS size and benchmark. Fig. 3(a) shows that while the gap between the proposed DRL framework and Benchmark 4 widens as N increases, the proposed CSI-free DRL framework still performs within 25% of the best benchmark under full CSI. This is a significant result that illustrates the effectiveness of the proposed CSI-free framework.

Fig. 3(b) translates the median GRCD into the equivalent BER in the data transmission phase using (6). We find that the BER achieved with Algorithm 1 is comparable with the best benchmark for all values of N . Moreover, one order-of-magnitude BER improvement may be achieved using a moderately-sized IRS with $N = 64$, which is a significant gain over the best non-IRS benchmark.

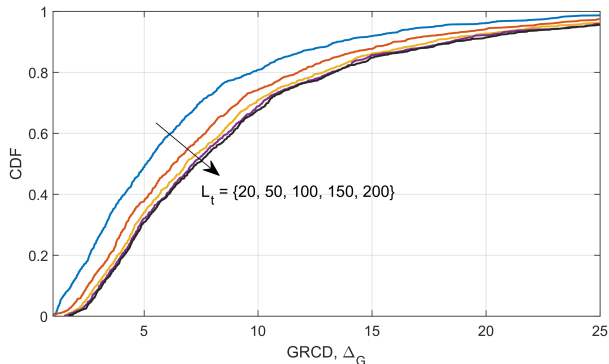


Fig. 4: Effect of training symbol duration on the GRCD.

Fig. 4 shows the effect of the training symbol duration L_t in the training phase on the quality of the solution obtained using Algorithm 1, where $N = 64$. One may observe that the GRCD obtained under small L_t is fairly poor, due to the inaccurate estimation of the channel covariance matrices based on few signal samples. With the added IRS, the number of channels in the system implicitly captured in each observation of \mathbf{C}_0 and \mathbf{C}_1 increases from $2M + 1$ to $MN + 2(M + N) + 1$. Thus, longer symbols are required for accurate estimation. Favorable performance is achieved once L_t becomes moderately large (e.g., $L_t = 100$), beyond which diminishing returns are ob-

served. These results suggest that a fairly accurate covariance estimation may be achieved when L_t reaches a certain level compared to the total number of implicitly observed channels. It should be noted that long training symbols are needed only in the training phase. Once a satisfactory set of $\{\mathbf{g}, \Theta\}$ is obtained, the data symbol duration can be reduced without affecting the GRCD.

V. CONCLUSION

In this letter, we utilized the unique characteristics of the IRS to improve the detection performance of an AmBC system. Under unknown CSI and ambient signal, we proposed a DRL-based framework to determine the reader's beamforming vector and the IRS reflection coefficients based on actual signal observations. The lack of CSI and varying reward function in each episode were mitigated with independent training in each episode and zero discount factor. Moreover, we utilized the optimal eigenvector combiner without IRS as initialization for each DRL step to encourage favorable exploration. Our results indicated that the DRL framework is capable of similar performance compared to various full-CSI benchmarks.

REFERENCES

- [1] G. Yang, Y. Liang, R. Zhang, and Y. Pei, "Modulation in the air: Backscatter communication over ambient OFDM carrier," *IEEE Trans. Commun.*, vol. 66, no. 3, pp. 1219–1233, Mar. 2018.
- [2] M. Hesson *et al.*, "Netscatter: Enabling large-scale backscatter networks," in *Proc. USENIX Symp. Netw. Sys. Design Impl. (NSDI 19)*, Feb. 2019, pp. 271–284.
- [3] H. Guo, Q. Zhang, S. Xiao, and Y. Liang, "Exploiting multiple antennas for cognitive ambient backscatter communication," *IEEE Internet Things J.*, vol. 6, no. 1, pp. 765–775, Feb. 2019.
- [4] S. Ma, G. Wang, R. Fan, and C. Tellambura, "Blind channel estimation for ambient backscatter communication systems," *IEEE Commun. Lett.*, vol. 22, no. 6, pp. 1296–1299, Jun. 2018.
- [5] W. Zhao, G. Wang, S. Atapattu, T. A. Tsiftsis, and X. Ma, "Performance analysis of large intelligent surface aided backscatter communication systems," *IEEE Wireless Commun. Lett.*, pp. 1–1, 2020.
- [6] M. Nemati, J. Ding, and J. Choi, "Short-range ambient backscatter communication using reconfigurable intelligent surfaces," in *Proc. IEEE Wireless Commun. Netw. Conf. (WCNC)*, 2020, pp. 1–6.
- [7] Ö. Özdogan, E. Björnson, and E. G. Larsson, "Intelligent reflecting surfaces: Physics, propagation, and pathloss modeling," *IEEE Wireless Commun. Lett.*, vol. 9, no. 5, pp. 581–585, May 2020.
- [8] Q. Wu and R. Zhang, "Intelligent reflecting surface enhanced wireless network via joint active and passive beamforming," *IEEE Trans. Wireless Commun.*, vol. 18, no. 11, pp. 5394–5409, Nov. 2019.
- [9] H. Chen, G. Yang, and Y. C. Liang, "Joint active and passive beamforming for reconfigurable intelligent surface enhanced symbiotic radio system," *IEEE Wireless Commun. Lett.*, pp. 1–1, 2021.
- [10] C. Huang, R. Mo, and C. Yuen, "Reconfigurable intelligent surface assisted multiuser MISO systems exploiting deep reinforcement learning," *arXiv preprint arXiv:2002.10072*, 2020.
- [11] A. Taha, Y. Zhang, F. B. Mismar, and A. Alkhateeb, "Deep reinforcement learning for intelligent reflecting surfaces: Towards standalone operation," *arXiv preprint arXiv:2002.11101*, 2020.
- [12] K. Feng, Q. Wang, X. Li, and C. Wen, "Deep reinforcement learning based intelligent reflecting surface optimization for MISO communication systems," *IEEE Wireless Commun. Lett.*, vol. 9, no. 5, pp. 745–749, May 2020.
- [13] J. Qian, F. Gao, G. Wang, S. Jin, and H. Zhu, "Noncoherent detections for ambient backscatter system," *IEEE Trans. Wireless Commun.*, vol. 16, no. 3, pp. 1412–1422, Mar. 2017.
- [14] G. Wang, F. Gao, R. Fan, and C. Tellambura, "Ambient backscatter communication systems: Detection and performance analysis," *IEEE Trans. Commun.*, vol. 64, no. 11, pp. 4836–4846, Nov. 2016.
- [15] T. P. Lillicrap *et al.*, "Continuous control with deep reinforcement learning," *arXiv preprint arXiv:1509.02971*, 2015.

[16] Y. Yang, B. Zheng, S. Zhang, and R. Zhang, “Intelligent reflecting surface meets OFDM: Protocol design and rate maximization,” *IEEE Trans. Commun.*, vol. 68, no. 7, pp. 4522–4535, 2020.